Rate-limiting step of the deuterium desorption kinetics from Zircaloy-4 oxidized in PWR light primary water

C. Juillet, Marc Tupin, Frantz A. Martin, François Jomard, Quentin Auzoux, Clément Berthinier, Fabrice Gaudier

Rate-limiting step of the deuterium desorption kinetics from Zircaloy-4 oxidized in PWR light primary water

C. Juillet[(1)], M. Tupin[(2)], F. Martin[(1)], F. Jomard[(3)], Q. Auzoux[(1)], C. Berthinier[(4)], F. Gaudier[(5)]

(1) Université Paris-Saclay, CEA, Service de la Corrosion et du Comportement des Matériaux dans leur Environnement, 91191, Gif-sur-Yvette, France.

(2) Université Paris-Saclay, CEA, Service d'Etude des Matériaux Irradiés, 91191, Gif-sur-Yvette, France.

(3) Université Paris-Saclay, UVSQ, CNRS, GEMaC, 78000, Versailles, France.

(4) Université Paris-Saclay, CEA, Service d'Etude Mécaniques et Thermiques, 91191, Gif-sur-Yvette, France.

(5) Université Paris-Saclay, CEA, Service de Thermohydraulique et de Mécanique des Fluides, 91191, Gif-sur-Yvette, France.

Keywords: Deuterium; Desorption kinetics; Zirconium alloys; Secondary Ion Mass Spectrometry; Numerical modelling

1 Abstract

This study aims at identifying the rate-limiting step and quantifying the kinetic constants of diffusion and deuterium desorption from a Zircaloy-4 alloy oxidized in light primary water. Secondary Ion Mass Spectrometry deuterium concentration profiles in ZrO_2, combined with finite elements simulations, reveal that the deuterium desorption from an oxidized Zircaloy-4 alloy is kinetically controlled by a mixed regime of surface recombination and diffusion in the oxide in the 600 K – 1000 K temperature range. At lower temperatures, desorption is controlled by the deuterium diffusion in the oxide layer whereas at higher temperatures the surface recombination reaction dominates.

2 Introduction

The nuclear pressurized water reactor (PWR) fuel claddings contain hydrogen originating from the manufacturing process and from the corrosion by water. Under normal operating conditions in PWRs, the outer surface of zirconium alloy fuel claddings is exposed to primary water and zirconium alloys continuously oxidize into zirconia. During this process, the cladding absorbs a fraction of the hydrogen produced by the reduction of water [1–3]. Hydrogen chemical potential and transport properties differ in zirconia and in the alloy, which leads to a partition of hydrogen between the alloy and the oxide scale. In the uranium oxide fuel, ternary fission leads to the formation of another hydrogen isotope: tritium. A part of this tritium is then absorbed and diffuse through the cladding, potentially reaching the primary water. The inner surface of the cladding is also oxidized by initial residual water and by the uranium oxide [4]. During drying, transport, reprocessing or storage of used nuclear fuels, some hydrogen and/or tritium may desorb from the cladding involving safety concerns. The present study aimed at quantifying the influence of the oxide scale on the tritium desorption from the cladding for a better estimation of the potential tritium release in the different aforementioned cases.

The hydrogen or tritium release from the bulk alloy has been decomposed into five steps, as detailed in [5–7]. The first step is the hydrogen diffusion through the α-Zr matrix generally via interstitial sites [8] towards the metal/oxide interface. Numerous studies on this process in the literature allow to estimate a hydrogen diffusion coefficient in the zirconium alloys over a wide range of temperatures [9–16]. It is expressed following an Arrhenius-type law whatever the zirconium alloy considered. An average hydrogen diffusion coefficient is deduced from the literature [8,10–16]:

$$D_{i_m}^{diff} = D_{i_m}^{0\,diff} . \exp\left(-\frac{E_a}{RT}\right) = 10^{-7} . \exp\left(-\frac{35000}{RT}\right) \quad \text{m}^2\,\text{s}^{-1} \qquad \text{(Eq. 1)}$$

with $D_{i_m}^{0\,diff}$ including the migration entropy and the jump attempt frequency, E_a the migration enthalpy (in J mol^{-1}), T the temperature (in K) and R the ideal gas constant (8.314 J K^{-1} mol^{-1}). The hydrogen diffusion coefficient in the zirconium alloys is equal to 6×10^{-11} m² s^{-1} at 573 K.

Hydrogen absorption and desorption kinetics into/from oxidized zirconium alloys have been widely studied in the literature [6,11,17–25]. A barrier effect of the oxide layer was highlighted irrespective of the transport direction: absorption [21–26] or desorption [6,11,17–20,27]. Andrieu *et al.* [28,29] were interested in tritium permeation through Zircaloy-4 into primary water. For experiments carried out for 252 days at 619 K, they concluded that the tritium permeation rate-limiting step was the tritium transport through the oxide layer.

The hydrogen diffusion mechanism in the oxide layer has been widely investigated in literature. As shown in Figure 1, the experimental procedures used for diffusion assessment (absorption by water corrosion process or release process) significantly affect the values of the hydrogen diffusion coefficient in the oxide layer. These values compiled from literature data, for instance at 573 K, vary from 10^{-21} to 10^{-17} m^2 s^{-1} [16,18,25,30]. The hydrogen diffusion coefficients estimated in the zirconium oxide layers are always much lower than the ones estimated in the alloy.

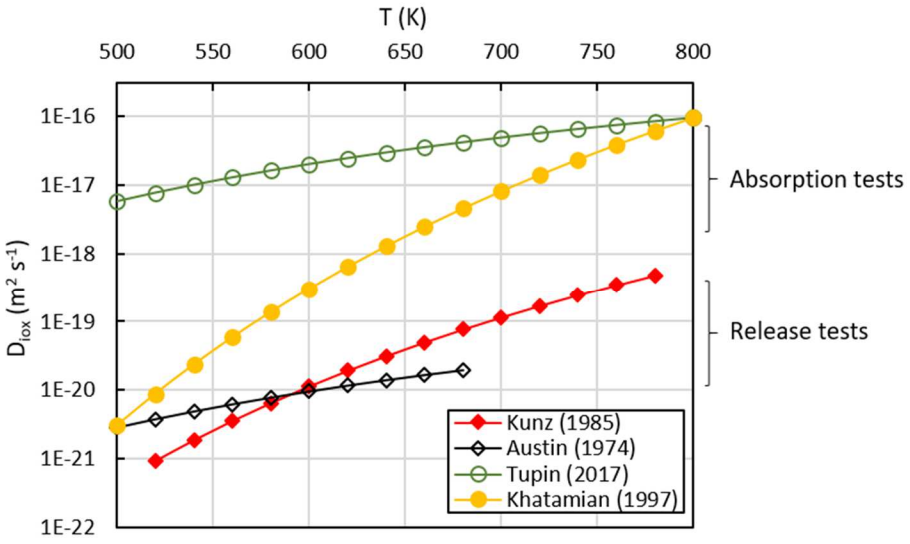

Figure 1. Evolution with temperature of some hydrogen diffusion coefficients in zirconium oxide layers compiled from literature *[16,18,25,30]*.

The values of the diffusion coefficients deduced from the release experiments gathered in Figure 1 are significantly lower (about two orders of magnitude at 633 K) than those obtained in absorption conditions. All the diffusion coefficients were determined by assuming that hydrogen diffusion through the oxide layer was the rate-limiting step. This striking gap may be explained by a different mechanism, a different rate-limiting step or a different hydrogen diffusing species between the absorption and release processes. More specifically the role played by the surface dissociation or recombination step has to be investigated from a kinetic viewpoint.

Moreover, an oxide scale dissolution into the alloy has been reported by Andrieu *et al.* [28,29] and Juillet *et al.* [6] during a long isothermal treatment or a temperature ramp, respectively. The difference of oxygen chemical potential between the oxide and the metal causes this dissolution, which is enhanced by the high oxygen solubility in zirconium [31]. Our previous study [6] on the hydrogen desorption from the Zircaloy-4 during a temperature ramp after oxidation in a dry Ar-20%O_2 atmosphere demonstrated that hydrogen desorption only began after local oxide layer dissolution

occurred. This means that, in such conditions, the hydrogen desorption from the alloy was controlled by the oxide dissolution kinetics. However, under the conditions encountered by fuel claddings in PWR primary water (long-term isotherms, temperature around 573 K), there is no actual oxide thickness decrease because of the continuous oxidation.

The aims of this study are to identify the rate-limiting step and to quantify the kinetic constants of diffusion and deuterium (^2H) desorption from a primary water-oxidized Zircaloy-4 alloy. To minimize the oxide layer dissolution throughout the experiment duration and to be closer to PWR operating conditions, the deuterium desorption kinetics were carried out under isothermal operating conditions. The adopted approach consisted of 4 main steps: (i) charging in hydrogen or deuterium the zirconium alloy (Zircaloy-4 here), then (ii) oxidizing these specimens in light primary water, (iii) carrying out isothermal desorption steps under vacuum, then (iv) comparing the experimental results with numerical simulations (Cast3M code [32] and URANIE platform [33]).

3 Experimental Procedure

3.1 Material and specimen preparation

Framatome supplied a 0.45-mm thick sheet of recrystallized Zircaloy-4 alloy for the present study (see chemical composition in Table 1). The specimens (1 x 1 cm) were ground up to grade P2000 with SiC emery paper then cleaned in deionized water, rinsed in acetone-ethanol solution and finally dried in air. A 0.35-mm final thickness was obtained.

Table 1. Chemical composition of the studied Zircaloy-4 ingot.

Alloying elements	Fe (wt.%)	Cr (wt.%)	Sn (wt.%)	O (wt.%)	C wt.ppm	Zr
Zircaloy-4	0.19 – 0.21	0.11	1.31 – 1.35	0.11 – 0.12	118 – 129	Bal.

3.2 Hydrogen and deuterium cathodic charging

Deuterium was chosen as an isotopic tracer in order to distinguish between hydrogen species present in the alloy before oxidation (both deuterium and hydrogen) from that absorbed during the oxidation experiments (hydrogen only). The cathodic charging device consisted of a platinum counter electrode serving as an anode and the sample to be charged acting as a cathode. The solution used was sulphuric acid H_2SO_4 at 0.05 mol L^{-1} in a mixture of D_2O and H_2O. To enhance the protons reduction, a cathodic

current density of -7.5 mA cm^{-2} was imposed by a galvanostat at the working electrode. Charging was done at 353 K and lasted 11 h. In order to homogenize the distribution of hydrogen and deuterium in the samples an annealing treatment was carried out in vacuum (10^{-7} mbar) at 673 K during 5 hours. The resulting hydrogen and deuterium concentrations before oxidation were quantified by thermal desorption spectrometry (TDS). They were [^{1}H] = 56 wt.ppm (i.e. 0.51 at.%) and [^{2}H] = 54 wt.ppm (i.e. 0.25 at.%). Such deuterium concentration therefore corresponds to a 27 wt.ppm equivalent hydrogen concentration.

3.3 Corrosion tests

The pre-charged Zircaloy-4 samples in hydrogen and deuterium were then corroded in a static autoclave at 633 K and 188 bars in light primary water up to 50 days to form an oxide thickness of 1.5 µm (deduced from the weight gain). The water chemistry was composed of 2 wt.ppm of lithium and 1000 wt.ppm of boron prepared using lithium hydroxide (LiOH, H_2O) and boric acid (H_3BO_4).

3.4 Thermal Desorption Spectrometry (TDS)

The Thermal Desorption Spectrometry technique was used to determine the hydrogen and deuterium content and the desorption kinetics of the pre-charged samples. Each specimen was inserted in a quartz tube under secondary vacuum (10^{-6} – 10^{-7} mbar), surrounded by a cylindrical furnace, coupled to a Transpector 100-M (INFICON™) quadrupole mass spectrometer. During heating, desorbed species are ionized, separated, detected and counted by the mass spectrometer. To convert the ion current into hydrogen and deuterium molar fluxes, calibrated $^2H_2$ leaks from LacoTech™ were used. The amounts of hydrogen and deuterium desorbed from the specimen in the TDS in the course of a temperature ramp of 10 K min^{-1} up to 1273 K were estimated by integration of the calibrated signals (m/z=3 and m/z=4) as function of the time during the experiment. After oxidation, one sample was desorbed in the TDS set-up at 773 K during 7 days and another at 723 K during 19 days. Under these desorption conditions, the mass spectrometer could not measure properly any desorption flux due to a high background noise compared to the potentially very low desorption flux. After each vacuum isotherm, the sample was cut into two parts: one part underwent a TDS temperature ramp of 10 K min^{-1} up to 1273 K in order to quantify the hydrogen and deuterium concentrations remaining in the specimen after 7 days at 773 K and 19 days at 723 K; the second one was used for further characterization by SIMS.

3.5 Secondary Ion Mass Spectrometry (SIMS)

SIMS analyses were carried out on the specimens before and after both desorption experiments, i.e. at 773 K during 7 days and at 723 K during 19 days. The Secondary Ion Mass Spectrometry system was a CAMECA IMS 7f and analysis conditions used a 40 nA current and 15 kV energetic Cs^+ primary ion beam. Two type of analyses were conducted:

- Penetration profiles of deuterium (^2H) and oxygen (^{16}O) from the surface were measured in dynamic sputtering conditions. The diameter of the analyzed area was 33 µm. Species depth distribution profiles were then deduced knowing the oxide thickness. The metal/oxide interface was set at 50 % of the ^{16}O signal maximum in zirconia. The different elements intensities were normalized by a multiplying factor in order to get the same ^{16}O signal intensity value in the oxide scale for each analysis.
- Ion mappings of the ^1H and ^2H elements distribution on a surface of 400 x 400 µm² were recorded. In this case, the samples were prepared in cross section embedded in a Wood alloy.

Figure 2 shows on a three-dimensional sample the locations where the SIMS profiles and maps were done.

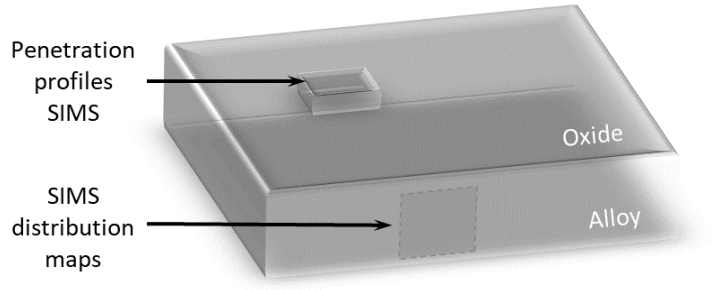

Figure 2. 3D schematic description of the location where the SIMS profiles and maps were done.

4 Experimental results

4.1 Estimation of the amount of deuterium desorbed from PWR-pre-oxidized specimens during the isothermal heat treatments

The hydrogen and deuterium desorption from oxidized samples were carried out under vacuum in the TDS set-up during 7 days at 773 K or 19 days at 723 K. These desorption conditions were chosen in

order to find the best time-temperature compromise, between a reasonable test duration (several days) and temperatures high enough to accelerate the desorption process while limiting the oxide layer dissolution [6,28,29].

The deuterium and hydrogen desorbed amounts were deduced from the quantities remaining in the material measured from a TDS temperature ramp test carried out after each isothermal test, the initial amount in each specimen before the oxidation step being known. Hydrogen and deuterium contents at the different steps of the experiments are summarized in Table 2**.** The hydrogen desorption flux obtained from a TDS temperature ramp after a 7-day isotherm at 773 K is presented on the Figure 3 as an example. The hydrogen and deuterium concentration values are quantified by integrating the desorption fluxes of H_2, HD and D_2 as function of time.

Table 2. Hydrogen and deuterium concentrations in the specimens after cathodic charging (measurements carried out after homogenization and before oxidation) and after isothermal desorption at 773 K and 723 K.

	Initial	After 7 days at 773 K	After 19 days at 723 K
[H] (wt.ppm H)	56	82	93
[D] (wt.ppm H)	27	31	30

** at.ppm = wt.ppm H x 91.22*

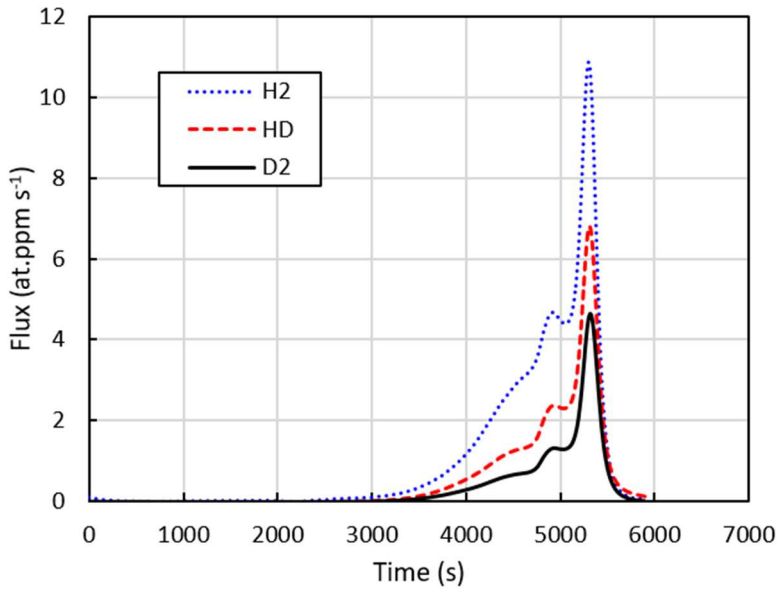

Figure 3. TDS flux of H_2 (blue dotted line), HD (red dashed line) and D_2 (black continuous curve) obtained for a temperature ramp of 10 K min^{-1} on a sample previously desorbed during 7 days at 773 K.

Irrespective of the thermal treatment, the pre-charged deuterium did not apparently desorb. The mass spectrometer does not measure any desorption flux because the signal is either zero or less than the device's detection limit. After the desorption step, the hydrogen concentrations within the metal rise by around 50 percent in comparison to the hydrogen amount initially present. This increase in ^{1}H content is due to the hydrogen (^{1}H) absorption during the oxidation step in light primary water. This hydrogen uptake of around 30 wt.ppm during the oxidation process is consistent with the work of Tupin *et al.* [25] who measured an absorption of 24 wt.ppm in 0.45-mm thick Zircaloy-4 alloy after 50 days of oxidation at 633 K and 187 bar in PWR solution ([B] = 1000 wt.ppm and [Li] 2 wt.ppm) to form an oxide thickness of 1.5 µm.

In order to characterize the hydrogen and deuterium localization in the metal, SIMS analyses were carried out before and after the isothermal desorption steps. The results of these analyses will be also compared with the ^{1}H and ^{2}H amounts previously measured by TDS.

Due to the highly heterogeneous distribution of hydrogen species in the metal (due to hydrides formation), local analyses such as SIMS abrasion profiles were not accurate. Thus, mappings of the ^{1}H and ^{2}H elements distribution in the metal were performed on the samples prepared in cross section before and after the desorption step, imaging ion distribution on 300×300 µm² areas (see Figure 4). On each map, for ^{1}H and ^{2}H elements, the signal was integrated into a region of interest (in red dotted lines in Figure 4, 250×250 µm² in area) in order to determine an average intensity of hydrogen or deuterium signal in cts s^{-1}. This average value is indicated in Figure 3 under each map obtained from ten scans of the area of interest.

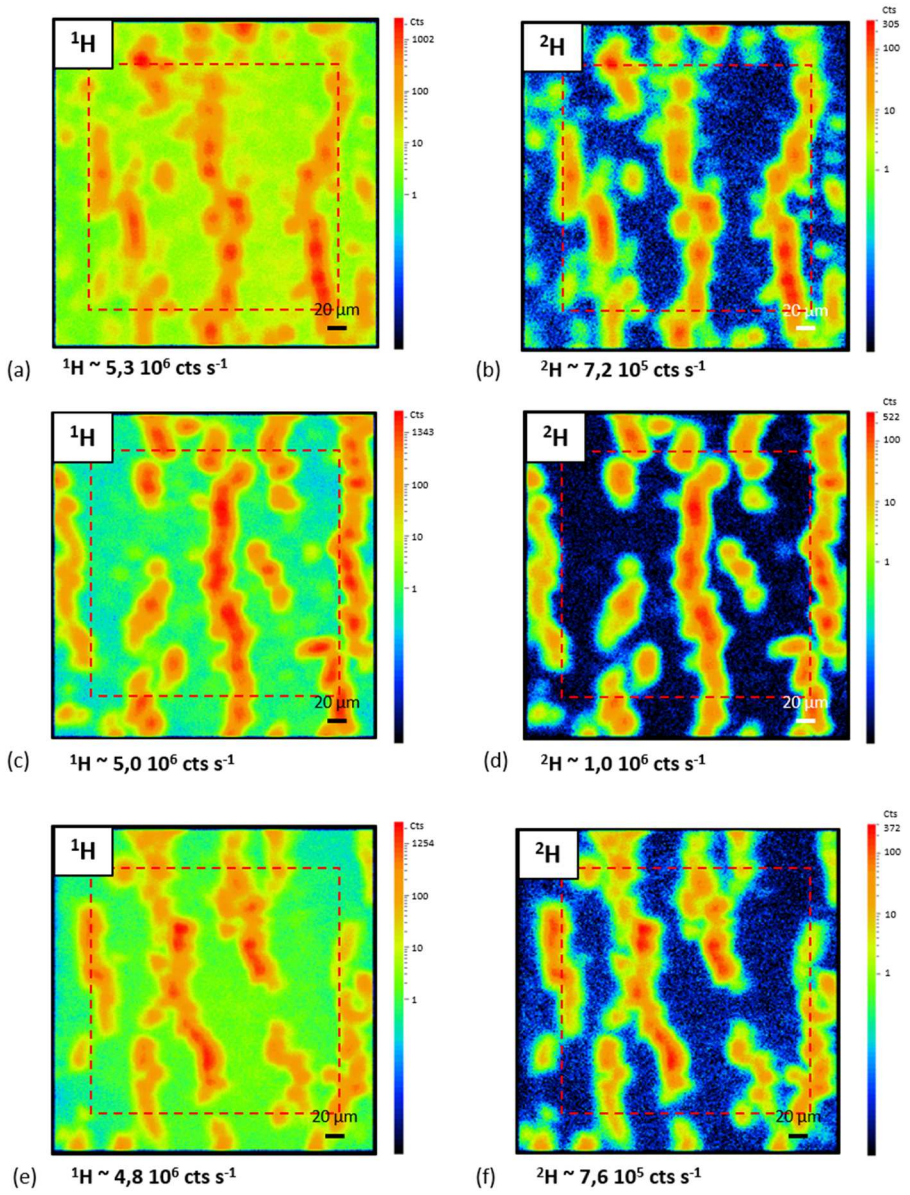

Figure 4. Mapping of the ^{1}H (left) and ^{2}H (right) elements distribution in the metal of Zircaloy-4 samples after cathodic charging followed by oxidation during 50 days in light primary water: (a-b) before desorption; (c-d) after desorption at 773 K during 7 days and (e-f) after desorption at 723 K during 19 days.

On the ion maps in Figure 4, the red color indicates a high concentration of the studied elements (^{1}H, ^{2}H). These maps reveal the presence of hydrides rich in hydrogen and deuterium for the three samples. A non-zero signal of hydrogen (^{1}H) in the matrix (green color in Figures 4a, 4c and 4e) may result from the hydrogen re-deposition process occurring during the analysis.

It is worth noting that, both the size of the zone analyzed by SIMS and the heterogeneity of the hydrogen distribution induced by the presence of hydrides may affect the accuracy of these SIMS-mapping measurements. A preliminary comparison between three ion maps recorded at three different zones of the same cross section allowed to estimate the accuracy of these SIMS-mapping to

be around 20 %. The deuterium intensity of the non-desorbed specimen (Figure 3b) thus basically ranges from 5.8 x 10^5 to 8.6 x 10^5 cps s^{-1}. Taking this 20 % accuracy into account, it can be assessed that the amounts of ^1H and ^2H before and after the isothermal desorption treatments remained equivalent, in consistency with previous TDS results.

To summarize, no or few deuterium present in the alloy was desorbed during the vacuum heat treatments carried out during 7 days at 773K and 19 days at 723K. This observation highlighted that the deuterium desorption is rate-limited by a very slow step such as the deuterium diffusion through the oxide layer or the surface recombination. Further analyses were needed to understand this extremely low desorption kinetics. SIMS abrasion analyses from the oxidized surface were performed on the three samples to track the hydrogen and deuterium diffusion process in the oxide layer.

4.2 Evolution of the deuterium distribution in the oxide scale during desorption heat treatments

These SIMS analyses aimed at providing information on the rate-limiting step of hydrogen desorption from the metal. For instance, a high concentration of deuterium in the oxide layer at the vicinity of the surface would reflect a kinetic control by the surface recombination step, while a deuterium concentration profile in zirconia from the oxide/alloy interface with a low penetration distance in the oxide would suggest a diffusion rate-limiting step. Please note that only deuterium (^2H) is used here, not hydrogen (^1H) due to its mixed origin (primary water or initial cathodic charging).

Figure 5 compares the normalized SIMS profiles of oxygen and deuterium for all samples before and after the isothermal desorption step.

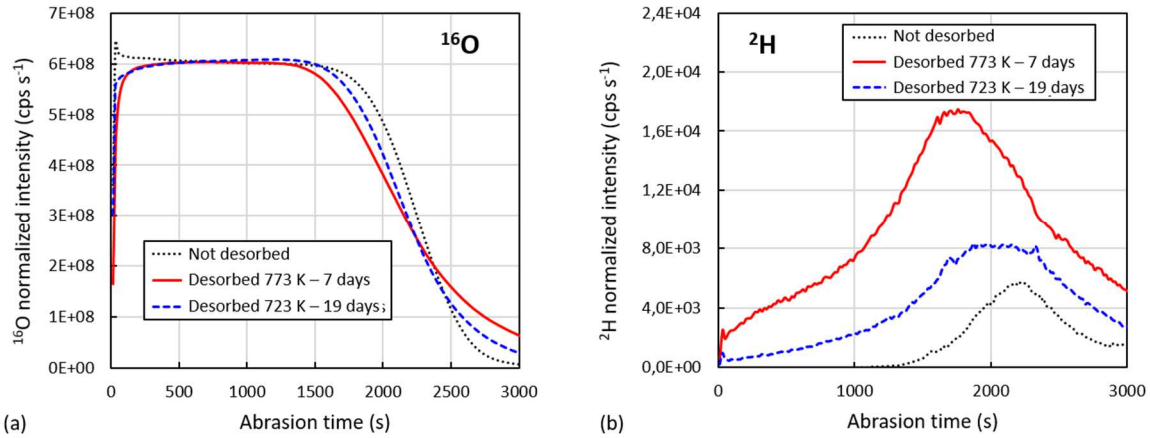

Figure 5. Normalized SIMS profiles after oxidation and before desorption (black dotted curves), after desorption at 773 K during 7 days (red continuous curves) and after desorption at 723 K during 19 days (blue dashed curves) of: (a) oxygen (^{16}O) and (b) deuterium (^{2}H).

In the case of a Zircaloy-4 alloy oxidized in light primary water and desorbed under isothermal conditions at 773 K or 723 K, the oxide scale dissolution is not very marked as evidenced by the oxygen intensities before and after desorption (Figure 5a). The oxide / alloy interface (50 % of the ^{16}O maximum signal) is indeed fluctuating between 2200 and 2300 s abrasion time, fluctuations that represent 5 % of the oxide layer thickness, i.e. around 75 nm as the layer thickness is 1.5 µm. A slight interface spreading is nonetheless observed. The oxide dissolution in the metal being low, it will be neglected thereafter. We also observe in Figure 4b that the deuterium concentration is undetectable in the core of the oxide layer after oxidation and before desorption (0 to 1000 s of abrasion in Figure 5b), and that some diffusion of deuterium from the metal occurred during the oxidation process (concentration gradient in the 1000 – 2000 s abrasion time).

In both studied desorption conditions, the deuterium present in the metal crossed the oxide/metal interface and diffused towards the surface, as evidenced by the concentration gradients in Figure 4b. An interesting point is that the deuterium intensity at the oxide/metal interface is significantly higher after desorption at 773 K than after desorption carried out at 723 K. The interfacial equilibrium constant between the deuterium concentrations in the oxide and in the metal depends on temperature. It is therefore very likely that the deuterium concentration in the oxide at the interface, in equilibrium with the deuterium concentration in the alloy, increases with temperature. Another striking point is the non-zero signal for deuterium (Figure 4b) observed at the vicinity of the surface after the isothermal desorption treatments: this indicates that deuterium (i) has arrived at the surface (via diffusion, as shown by the concentration profile), and (ii) has accumulated in the subsurface of the oxide layer, suggesting a mixed kinetic regime with two rate-limiting steps.

In order to determine the rate-limiting step(s) and to quantify the associated kinetic constants, these SIMS deuterium profiles after oxidation and desorption heat treatment were simulated using a numerical modelling with the finite elements (FE) Cast3M code. The corresponding model and simulations are presented in the next section.

5 Numerical model and simulation approach

5.1 Description of the modelling with Cast3M code

Finite Elements calculations may diverge when one of the simulated parameters is subjected to local discontinuities. Therefore, the numerical model developed with the Cast3M code assumes for all times that the hydrogen concentrations in the metal and the oxide are equal at the metal/oxide interface. In other words, the equilibrium constant at this interface is considered to be equal to 1.

For the same reason, this model merges the steps of subsurface/surface passage and surface recombination into a single step. This simplification of the reaction system imposed by the constraints of numerical modelling by finite elements means that the equilibrium constant of the subsurface/surface passage step is considered as included in the kinetic constant of the surface recombination.

Finally, the modelling of the numerical code takes only into account three steps as illustrated in Figure 6.

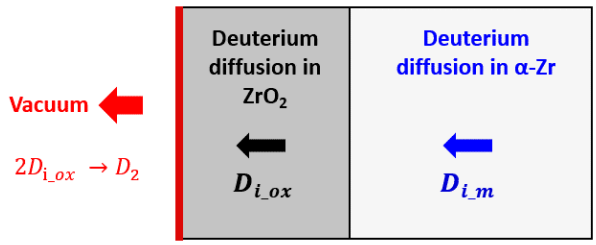

Figure 6. Sketch of the system considered for deuterium release from the alloy in the numerical study.

The diffusion equations in the alloy and in the oxide layer implemented in the model are governed by Fick's second law.

$$\frac{\partial C_{D_{i\_m}}}{\partial t} = \vec{\nabla} \cdot \left(D_{i_m}^{diff} \overrightarrow{\nabla \left(C_{D_{i\_m}} \right)} \right) \quad \text{(Eq.2)}$$

$$\frac{\partial C_{D_{i\_ox}}}{\partial t} = \vec{\nabla} \cdot \left(D_{i_{ox}}^{diff} \overrightarrow{\nabla \left(C_{D_{i\_ox}} \right)} \right) \quad \text{(Eq.3)}$$

with $C_{D_{i\_m}}$ the concentration of deuterium atoms in the interstitial position in the metal (mol m^{-3}), $C_{D_{i\_ox}}$ the concentration of deuterium atoms in the interstitial position in the oxide (mol m^{-3}), $D_{i_m}^{diff}$ and $D_{i_{ox}}^{diff}$ the deuterium diffusion coefficients in the metal and in the oxide, respectively (m^2 s^{-1}).

The expression (Eq.1) for the hydrogen diffusion coefficient in the metal is used as input data in the finite element code (Cast3M) for all the simulations. The hydrogen and deuterium diffusion coefficients in the α-Zr phase are assumed to be equivalent. The passage of deuterium from subsurface to oxide surface and the process of surface recombination and desorption in the form of dideuterium is described by reaction (R.1) and (R.2) respectively. The reaction (R.2) is forced in the forward direction by vacuum pumping, so equilibrium is not possible and the absorption reaction was neglected.

$$D_{i\_ox} + s \overset{K_{eq\_sub}}{\longleftrightarrow} D_{\_s} \quad \text{(R.1)}$$

$$2D_{\_s} \xrightarrow{k_{recomb}} D_2 + 2s \quad \text{(R.2)}$$

where D_{i_ox} is a deuterium atom in the interstitial position in the oxide at the outer interface (mol m^{-3}), $D_{\_s}$ the deuterium atom adsorbed on the surface, s a free site on the surface and D_2 the molecule desorbed in vacuum, K_{eq_sub} the equilibrium constant of the reaction (R.1) and k_{recomb} the desorption rate constant of the reaction (R.2).

As previously mentioned, the code does not take into account the subsurface – surface passage step but consider the following surface recombination process (R.3) which is in reality the linear combination of the reactions (R.1) and (R.2):

$$2D_{i\_ox} \xrightarrow{k'_{des} = k_{recomb} \times K^2_{eq\_sub}} D_2 \quad \text{(R.3)}$$

Assuming the hydrogen subsurface – surface passage at the equilibrium, which means that this step is very fast compared with the recombination one, the desorption flux of deuterium (mol$_{D2}$ m^{-2} s^{-1}) is expressed by the following equation (Eq.4):

$$\varphi_{D_2} = k'_{des} \left(C_{D_{i\_ox\,|\,at\,x=0}} \right)^2 = \frac{k_{des}}{2C_{D_{i\_ox}}^{sat}} \left(C_{D_{i\_ox\,|\,at\,x=0}} \right)^2 \quad \text{(Eq.4)}$$

with $k'_{des} = \frac{k_{des}}{2C_{D_{i\_ox}}^{sat}}$.

k'_{des} is the desorption constant of the reaction (R.3) (m^4 mol_{D2}^{-1} s^{-1}), k_{des} is the desorption constant introduced into Cast3M code (m s^{-1}) and $C_{D_{i\_ox}}^{sat}$ is the saturation concentration of deuterium in the oxide layer (mol m^{-3}). $C_{D_{i\_ox}|\ at\ x=0}$ corresponds to the deuterium concentration at the subsurface. Finally the relationship between k_{des} and k'_{des} is the following equation (Eq.5):

$$k_{des} = 2C_{D_{i\_ox}}^{sat} k'_{des} \quad \text{(Eq.5)}$$

The concentration $C_{D_{i\_ox}}^{sat}$ is an input parameter in Cast3M. However, no accurate measure of this parameter value is available in literature.

The gradual decrease in oxygen signal intensity observed on SIMS profiles (Figure 4a) indicates that the metal/oxide interface is extended and diffuse. This is caused by the size of area analyzed by SIMS (33 µm in diameter) and the roughness of the inner interface. Contrary to the SIMS profiles, the 1D modelling with Cast3M code supposes a sharp interface between the oxide layer and the metal, which was assumed fixed and at a distance of 1.5 µm from the oxide surface.

In order to compare and calculate the difference between the simulated profiles and those obtained experimentally by SIMS analysis, the SIMS profiles were linearly extrapolated up to the metal/oxide interface. The extrapolated value of the deuterium intensity at this interface was converted to concentration, assuming that for the experiment at 773 K, the deuterium concentration in the oxide at the internal interface was equal to the initial concentration in the metal (150 mol m^{-3}). The hypothesis of the deuterium concentration equality at the metal/oxide interface is supported by two observations based on the work of Tupin *et al.* [34]. First, in their work, Tupin *et al.* observe from SIMS analyses on a Zircaloy-4 oxidized 28 days in D_2O at 633 K (2 wt.ppm of lithium and 1000 wt.ppm of boron), a hydrogen intensity in the zirconia resulting from the absorption from the metal or the residual hydrogen in the heavy water equivalent to the hydrogen intensity in the metal. Second, according to ERDA measurements, the hydrogen concentration in zirconia was determined around 2 at. %. From our SIMS analyses, the deuterium intensity was found to be ten times lower than the hydrogen intensity at the metal/oxide interface, which would assume a deuterium concentration at the metal/oxide interface of 0.2 at. %. As a reminder, a deuterium concentration equal to 150 mol m^{-3} corresponds to 0.3 at. %. Given the relation between the intensities linearly extrapolated at the interface obtained on the samples desorbed at 773 K during 7 days and at 723 K during 19 days, the deuterium concentration in the oxide (and in the metal) at the metal/oxide interface was deduced from the following formula :

$$C_{D_{i\_ox}}^{sat}(723K) = C_{D_{i\_ox}}^{sat}(773K)\left(I_{ext}^{723}/I_{ext}^{773}\right) \quad \text{(Eq.6)}$$

where I_{ext}^{723} and I_{ext}^{773} are the extrapolated intensity values at the metal/oxide interface for the desorption experiments at 723 and 773 K, respectively, and $C_{D_{i\_ox}}^{sat}(723K)$ and $C_{D_{i\_ox}}^{sat}(773K)$ are the deuterium concentration at the metal/oxide interface at 723 and 773K.

Finally, the deuterium concentration in the oxide was set at 80 mol m^{-3} for the experiment at 723 K. The initial deuterium profile before desorption was extended linearly in the metal until it reached the same deuterium concentration as for the desorbed samples, *i.e.* 80 mol m^{-3} at 723 K and 150 mol m^{-3} at 773 K.

Figure 6 describes the measured and extrapolated SIMS profiles of deuterium as a function of the distance from the oxide surface formed on the Zircaloy-4 samples oxidized in light primary water before (black crosses) and after desorption (red squares and blue triangles, respectively for 7 days at 773 K and 19 days at 723 K). Figure 8 shows the schematic representation of the deuterium concentration profile, extracted from the SIMS depth profiles shown in Figure 7 before deuterium desorption, which has been implemented in the numerical model as initial conditions. The deuterium intensity peak observed in the metal for the non-desorbed sample (black crosses) corresponds to the presence of a hydride which precipitated during cooling. Contrarily to the situation in the metal, the deuterium distribution measured in the oxide is considered to be identical to the one at the experiment temperature.

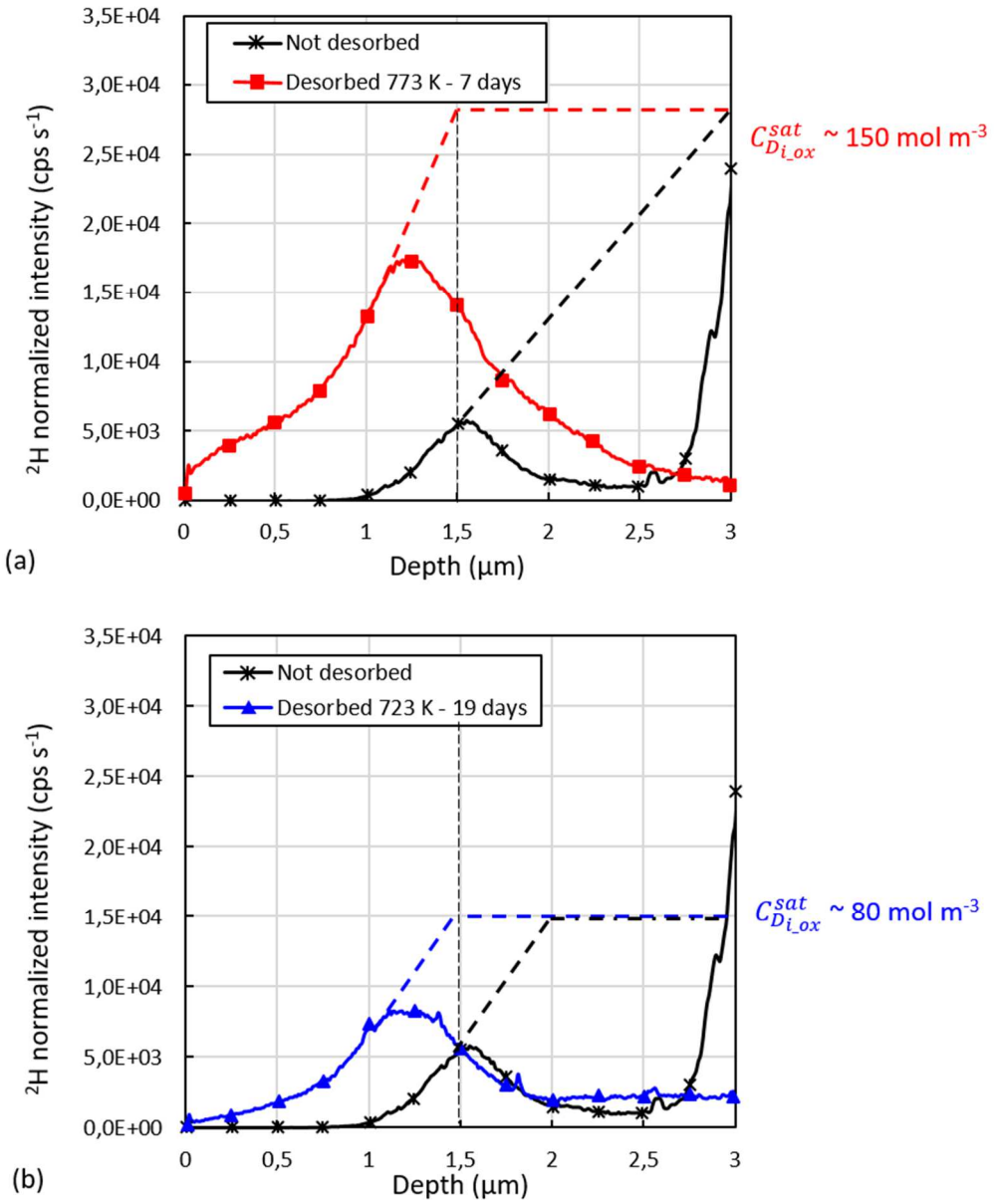

Figure 7. Normalized SIMS profiles as a function of depth after 50 days oxidation in light primary water at 633 K and before desorption (black crosses), (a) after desorption at 773 K during 7 days (red squares) and (b) after desorption at 723 K during 19 days (blue triangles) of deuterium: measured SIMS profiles (continuous lines) and extrapolated SIMS profiles (dashed lines).

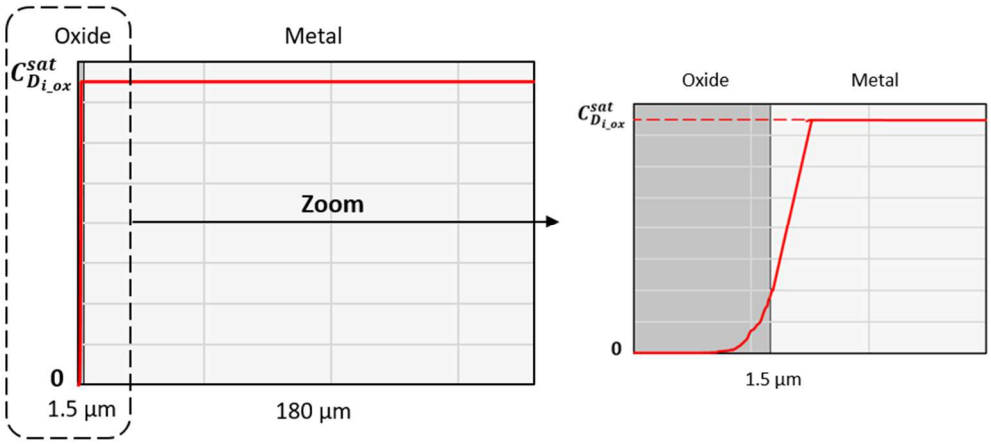

Figure 8. Schematic representation of the SIMS profile before desorption injected into the numerical model for a 1.5 µm-thick oxide layer, a 180 µm-thick metal and a saturation deuterium concentration dependent on the simulated experiment ($C_{D_{i\_ox}}^{sat}$= 150 mol m^{-3} or 80 mol m^{-3} depending on the considered temperature).

5.2 Calculations and optimization

It is assumed here, as generally admitted, that the desorption constant (k_{des}) and the deuterium diffusion coefficient in the oxide ($D_{i_{ox}}^{diff}$) depend on the temperature according to an Arrhenius law (Eq.7 and 8 respectively).

$$k_{des} = k_{des}^{0}.\exp\left(-\frac{Ea_{des}}{RT}\right) \quad \text{(Eq.7)}$$

$$D_{i_{ox}}^{diff} = D_{i_{ox}}^{0\ diff}.\exp\left(-\frac{Ea_{diff}}{RT}\right) \quad \text{(Eq.8)}$$

with k_{des}^{0} (m s^{-1}) and $D_{i_{ox}}^{0\ diff}$ (m^2 s^{-1}) the pre-exponential factors and Ea_{des} and Ea_{diff} the activation energies of desorption and migration in the oxide respectively (J mol^{-1}).

The previously defined kinetic parameters are used as input data in Cast3M code.

Coupling Cast3M with the URANIE platform makes the optimization of the values of these four kinetic parameters (k_{des}^{0}, $D_{i_{ox}}^{0\ diff}$, Ea_{des} and Ea_{diff}) possible. The Cast3M-URANIE coupling procedure is detailed in our previous paper [5]. A dot matrix with random quadruplet values with the Latin Hypercube Sampling methodology is generated by the URANIE sample tool. For each quadruplet of values and each desorption heat treatment (773 K during 7 days and 723 K during 19 days), the FE code (Cast3M) simulates the associated deuterium concentration profile as a function of depth. Using the following formula (Eq.9), the normalized squared difference between the simulated profiles and the experimental ones is calculated by Cast3M:

$$RR_i = \frac{\sum_j (F_{simu}(x_j) - F_{exp}(x_j))^2}{\max\left(\sum_k (F_{simu}(x_k))^2,\ \sum_l (F_{exp}(x_l))^2\right)} \quad \text{(Eq.9)}$$

with RR_i a partial error criterion for experiment "i", $F_{simu}(x_j)$ and $F_{exp}(x_l)$ the simulated concentration at the abscissa x_j and the experimental one at abscissa x_l, respectively. Subscript "i" (i ∈ {1;2}) refers to following experiments: {1} 773 K during 7 days, {2} 723 K during 19 days.

A total error criterion called RESULTAT has also been defined and corresponds to the sum of the RRi.

The ranges of investigation for each parameter are summarized in Table 3. The range of values for the desorption parameters were inspired by previous studies carried out at CEA. The range of values chosen for the diffusion coefficient of hydrogen in the oxide layer allow to cover the wide range of values provided by literature (from 10^{-21} to 10^{-16} m² s^{-1}) as previously shown in Figure 1 [16,18,25,30], in the temperature range of interest for the present study (i.e. 723 – 773 K).

Table 3. Investigation ranges of the kinetic parameters used in the numerical calculations.

$D_{i_m}^{diff}$ (m^2 s^{-1})	$\ln(k_{des}^0)$	Ea_{des} (kJ mol^{-1})	$\ln(D_{i_{ox}}^{0\ diff})$	Ea_{diff} (kJ mol^{-1})
$10^{-7}\exp\left(-\frac{35000}{RT}\right)$	(-25) – (-20)	30 – 50	(-18) – (-13)	150 – 180

The total error criterion RESULTAT reaches a minimum for the apparent desorption kinetic constant (k'_{des}) and a diffusion coefficient ($D_{i_{ox}}^{diff}$) equal to:

$$k'_{des} = 7x10^{-13}\ exp\left(-\frac{34{,}5\ kJ\ mol^{-1}}{RT}\right)\ m^4\ mol^{-1}\ s^{-1} \quad \text{(Eq.10)}$$

and

$$D_{i_{ox}}^{diff} = 2x10^{-8}\ exp\left(-\frac{156{,}1\ kJ\ mol^{-1}}{RT}\right)\ m^2\ s^{-1} \quad \text{(Eq.11)}$$

Figure 9 compares the simulated SIMS profiles with this apparent desorption kinetic constant (Eq.10) and this diffusion coefficient (Eq.11) with the measured and extrapolated experimental SIMS profiles.

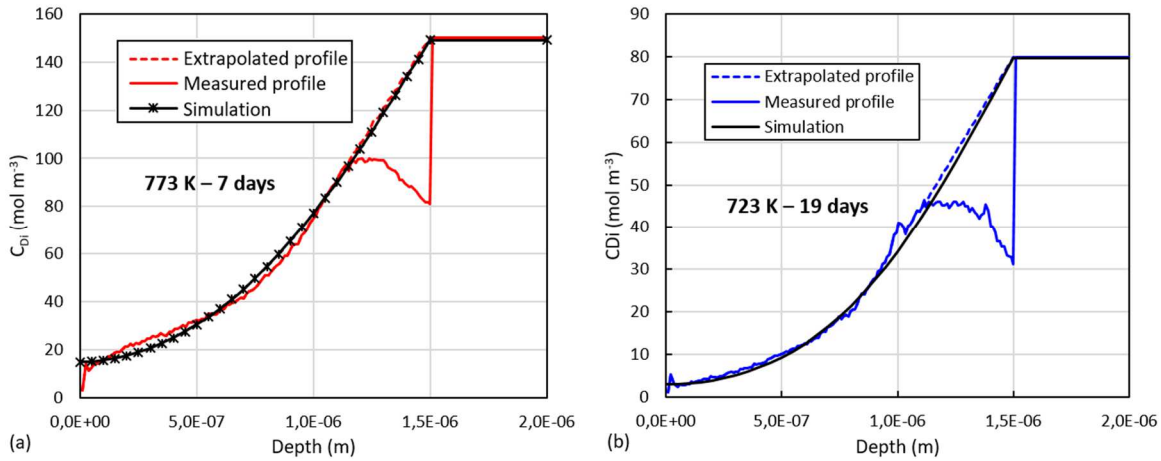

Figure 9. Measured experimental (continuous lines), extrapolated experimental (dotted lines) and simulated (black crosses) SIMS profiles of deuterium concentration as function of depth. Simulated profiles are drawn using kinetics constants Eq.10 and Eq.11: (a) after desorption at 773 K during 7 days and (b) after desorption at 723 K during 19 days.

On Figure 9, the simulations (black crosses in Figure 8) describe very well the SIMS profile after desorption at 773 K during 7 days and slightly underestimate the SIMS profile after desorption at 723 K during 19 days. A globally very good agreement between simulation and experimental data was achieved. However, as these kinetic constants was determined based on only two experiments, further (future) investigations would be needed to assess them more accurately.

As highlighted in Figure 10, the hydrogen diffusion coefficients in the oxide extracted during this work at 773K and 723K (blue crosses) are in good agreement with those stemming from the works of Kunz [18] and Austin [16]. These latter have been deduced from tritium release experiments from a Zircaloy-2 alloy oxidized and previously charged with tritium. On the other hand, the diffusion coefficients of this study are not consistent with the literature data obtained from absorption experiments (yellow and green circles). Many possibilities could explain this gap.

First of all, the mechanism of the hydrogen release from the metal is not necessarily the same as the one occurring during the hydrogen absorption process induced by the water corrosion. The hydrogen diffusing species can actually be different between absorption and release processes resulting in a significant variation of the migration energy and the hydrogen diffusion coefficient.

It can be also due to the modelling considered and its deficiencies. In the absorption study, Tupin *et al.* [25] simulate the hydrogen diffusion profile in the oxide layer to quantify the diffusion coefficient using Fick's second law without taking into account the adsorption reaction at the oxide surface. The

finite element model used in the present study considers in contrast the surface recombination reaction in addition to the diffusion process.

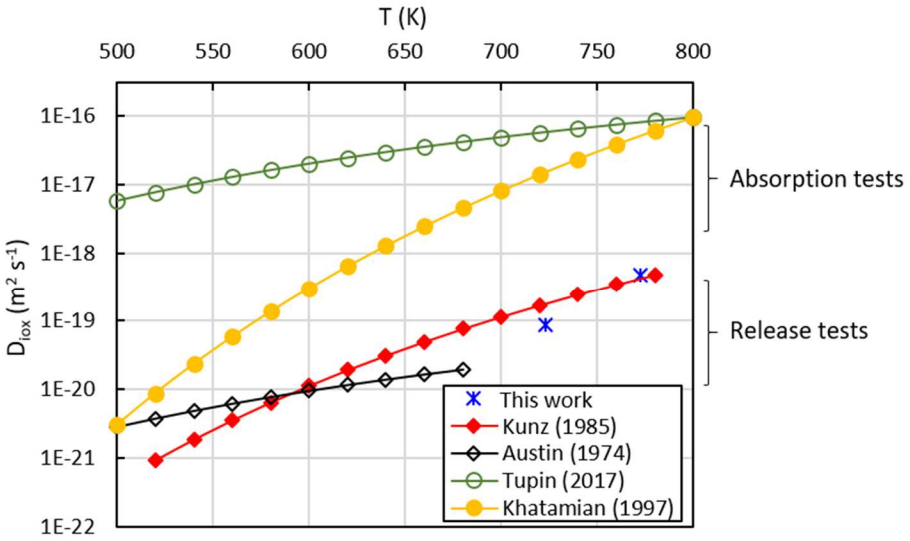

Figure 10. Comparison of the "hydrogen" (or its isotopes) diffusion coefficients in the oxide layer found in the present study (blue crosses) with literature-extrapolated values (versus experimental method) *[16,18,25,30]*.

Knowing the desorption kinetic constant and the diffusion coefficient, the deuterium desorption flux could be simulated. Figure 11 presents the deuterium desorption flux obtained by simulation at 773 K during 60 days.

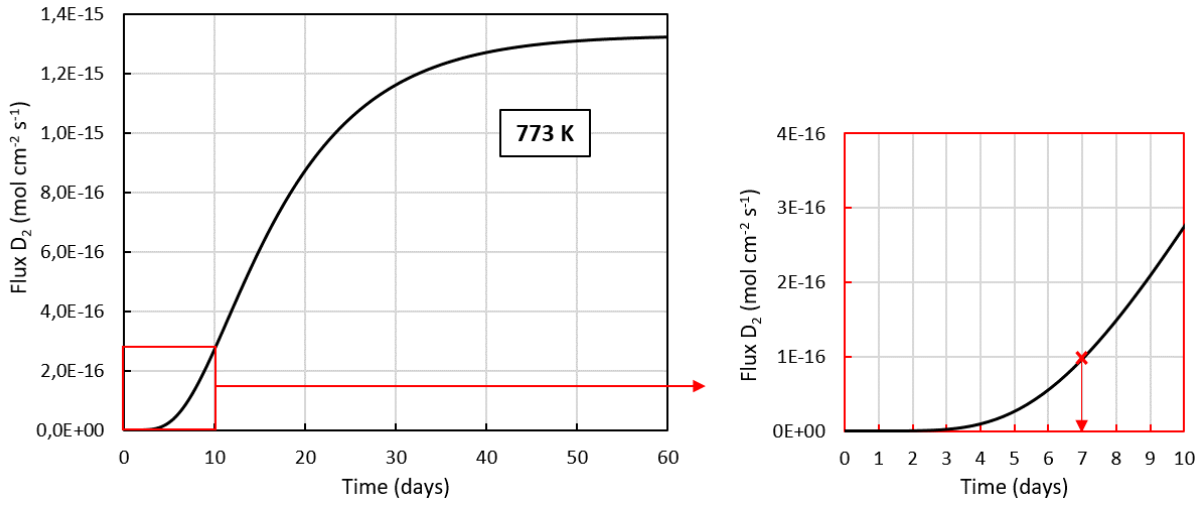

Figure 11. Simulated deuterium desorption flux at 773 K during 60 days with the kinetic constants expressed according to Eq.10 and Eq.11.

In agreement with the experimental SIMS profile in Figure 9a, Figure 11 shows that after 7 days at 773 K, the deuterium desorption flux is in a transient state. The higher the desorption time, the higher the deuterium desorption flux. This latter tends towards a constant value beyond 60 days of desorption meaning that the steady-state is reached. In view of the simulated desorption flux during the first 7 days, the deuterium desorbed amount is estimated to be in the order of 6 x 10^{-11} mol_{D2} cm^{-2}. Considering a 1 cm^2 surface sample with a 0.35 mm thickness comprising an initial deuterium concentration of 150 mol m^{-3}, only one thousandth percent of the initial amount is released after 7 days of vacuum treatment at 773 K. This desorbed deuterium quantity is actually not detectable with the techniques used in the present study (TDS and SIMS).

In PWRs, the operating temperature being lower (~ 573 K), the steady-state establishment will take longer. Moreover, in this context, the fuel cladding remains in the reactor for several months. It is therefore important to study the deuterium release in the long term when the steady-state should be reached.

5.3 Analysis of the calculations

5.3.1 Surface concentration at steady-state

In steady state, the deuterium diffusion flux arriving at the surface is equal to the desorption rate as expressed in the following equation (Eq.12):

$$\frac{D_{iox}^{diff}}{e_{ox}}\left(C_{D_{i_{ox_{int}}}} - C_{D_{i\_ox\_s-s\,|\,at\,x=0}}\right) = k'_{des}\left(C_{D_{i\_ox\_s-s\,|\,at\,x=0}}\right)^2 \quad \text{(Eq.12)}$$

equivalent to (Eq.13)

$$\left(C_{D_{i\_ox\_s-s\,|\,at\,x=0}}\right)^2 + \frac{D_{iox}^{diff}}{k'_{des}\,e_{ox}} C_{D_{i\_ox\_s-s\,|\,at\,x=0}} - \frac{D_{iox}^{diff}}{k'_{des}\,e_{ox}} C_{D_{i_{ox_{int}}}} = 0 \quad \text{(Eq.13)}$$

with $C_{D_{i\_ox\,int}}$, the deuterium concentration at the metal/oxide interface, $C_{D_{i\_ox\_s-s\,|\,at\,x=0}}$, the steady-state deuterium concentration at the outer interface (mol m^{-3}) and e_{ox} the oxide thickness equal to 1.5 µm.

Solving this second-degree equation in deuterium surface concentration gives the unique physical solution for the steady state deuterium surface concentration (Eq.14):

$$C_{D_{i\_ox\_s-s_{|\ at\ x=0}}} = \frac{-\frac{D_{i_{ox}}^{diff}}{k'_{des}\, e_{ox}} + \sqrt{\left(\frac{D_{i_{ox}}^{diff}}{k'_{des}\, e_{ox}}\right)^2 + 4\frac{D_{i_{ox}}^{diff}}{k'_{des}\, e_{ox}} C_{D_{i_{ox_{int}}}}}}{2} \qquad \text{(Eq.14)}$$

As already mentioned, the actual deuterium concentration in the oxide at the metal/oxide interface is not known. However, following the assumption of the equilibrium constant at the metal/oxide interface being equal to one, the calculated deuterium concentration in the oxide at the interface is the same as the one in the metal, whatever the temperature.

Figure 12 shows the evolution of the steady-state surface concentration of deuterium versus temperature.

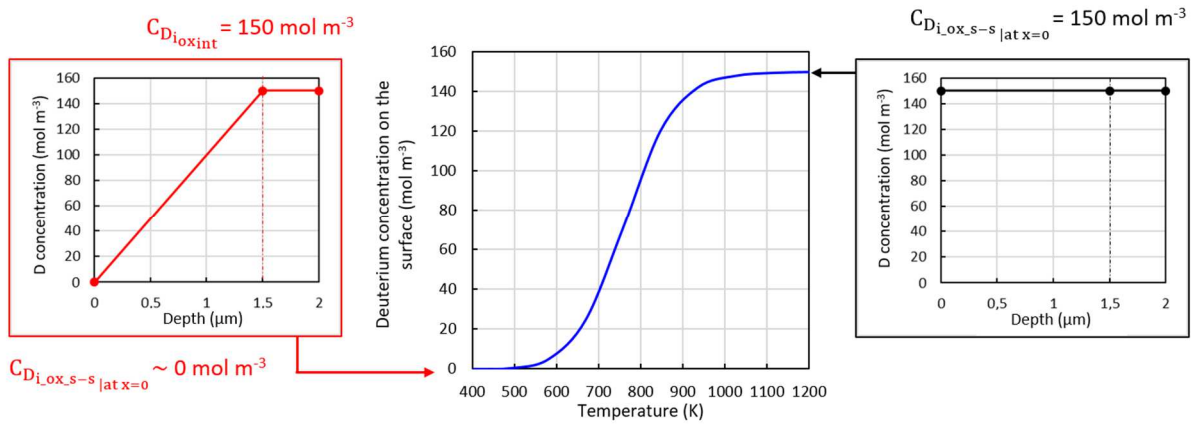

Figure 12. Evolution of the steady-state surface concentration of deuterium versus temperature with the concentration profiles associated to the deuterium in the oxide at 400 K (in red on the left) and at 1200 K (in black on the right), deuterium profiles for $C_{D_{i_{ox_{int}}}}$ = 150 mol m^{-3}.

Three domains are evidenced in Figure 12 (central blue curve):

1. At low temperatures, the deuterium release process is limited by diffusion through the oxide layer. In this case, a linear concentration gradient of deuterium is established between the inner to the outer interfaces and the surface concentration is low.
2. At high temperatures, the deuterium surface recombination is the rate-limiting step. The concentration is then uniform and constant throughout the oxide layer and close to the deuterium concentration at the metal/oxide interface.
3. For intermediate temperatures (typically in the [500; 1000] K range), the steady state surface concentration increases significantly with the temperature and the concentration gradient inside the oxide layer therefore decreases when temperature raises.

To summarize, the deuterium release process can be divided in three kinetic regimes as function of temperature: at low temperature, the rate-limiting step is the deuterium diffusion through the oxide; at high temperatures, deuterium surface recombination is rate-limiting and in-between a mixed kinetic regime prevails. These deductions from steady state analyses will be further discussed later on.

As shown in Figure 13, gathering the experimental concentration profiles extracted from SIMS analysis and the simulation of the steady-state concentration profile, it is clear that the steady-state has not been reached at the end of the 7-days desorption experiment at 773 K : the deuterium surface concentration is much lower than the calculated steady-state concentration.

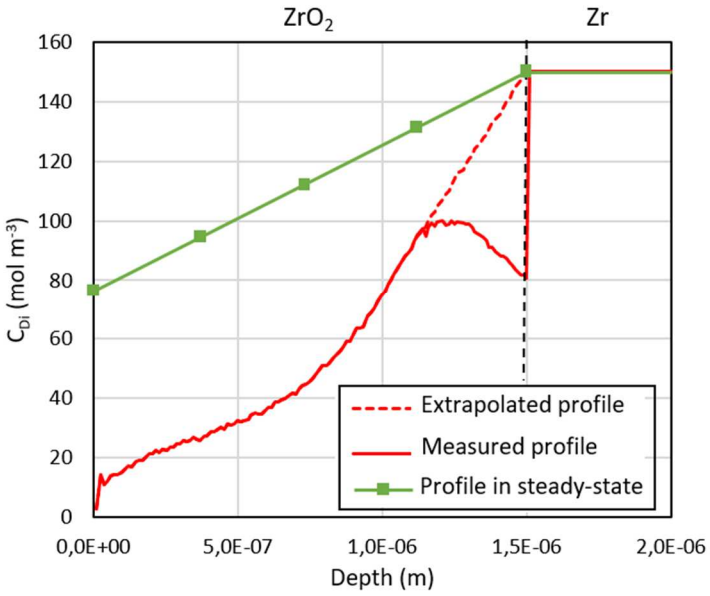

Figure 13. Comparison between measured (red continuous line) and extrapolated (dotted lines) experimental SIMS profiles of deuterium concentration as function of depth after 7 days of desorption at 773 K and the simulated (green squares) deuterium profile at the steady-state at 773 K.

The next section is dedicated to draw the evolution of the diffusion flux and the recombination rate as a function of temperature and to study the predominance domain of each process in terms of kinetic control.

5.3.2 Diffusion and surface recombination pure cases and rate-limiting regime versus temperature

Using the optimized kinetic constants of desorption and diffusion of deuterium in the oxide layer, the flux can be calculated for:

- **a surface recombination pure case** from (Eq.15):

$$\varphi_{D_2} = k'_{des}\left(C_{D_{i\_ox\,|\,at\,x=0}}\right)^2 \qquad \text{(Eq.15)}$$

where $C_{D_{i\_ox\,|\,at\,x=0}}$ is equal to 150 mol m^{-3} because there is no concentration gradient of deuterium in the oxide in a surface recombination pure case.

- **a diffusion pure case** according to (Eq.16):

$$\varphi_{D_2}^{diff} = \frac{D_{i_{ox}}^{diff}}{e_{ox}}\left(C_{D_{i_{ox_{int}}}} - C_{D_{i\_ox\,|\,at\,x=0}}\right) \qquad \text{(Eq.16)}$$

with $C_{D_{i\_ox\,|\,at\,x=0}}$ equals 0 mol m^{-3} and $C_{D_{i_{ox_{int}}}}$ equals 150 mol m^{-3}.

Figure 14 shows the temperature domains where the desorption flux according to the expressions of k'_{des} and $D_{i_{ox}}^{diff}$ determined previously is limited either by the deuterium diffusion in the oxide or by the surface recombination of deuterium into dideuterium. The deuterium desorption flux in steady-state and in transient state after 7 days at 773 K and 19 days at 723 K are compared.

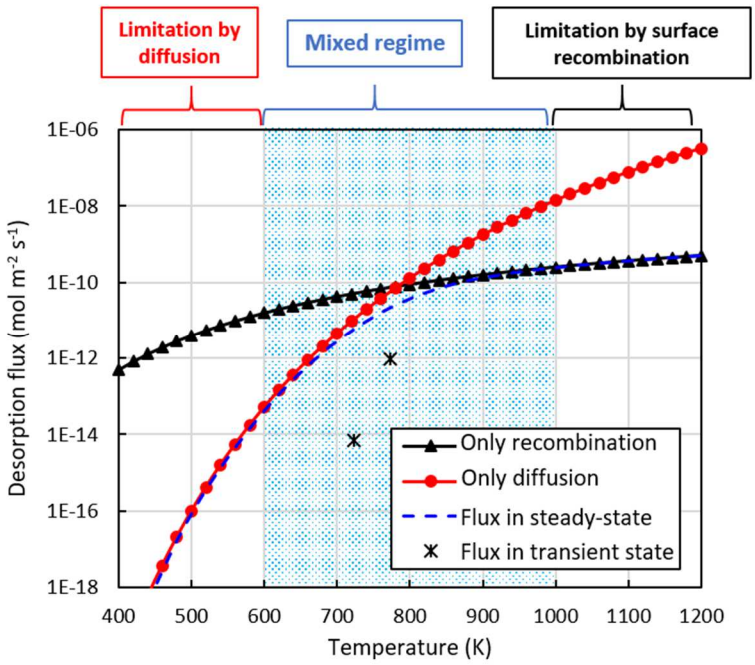

Figure 14. Desorption fluxes evolution as a function of temperature, considering diffusion as a limiting step (red circles) or the surface recombination reaction (black triangles), taken individually from the kinetic constants determined previously (Eq.10 and Eq.11) and the desorption flux in steady-state (blue dotted line) and in transient state (black crosses).

For relatively low temperatures, below 600 K, the deuterium desorption rate is controlled by hydrogen diffusion in the oxide layer. Above 1000 K, the surface recombination of the deuterium becomes limiting provided the oxide layer still exists. In the temperature range studied, *i.e.* between 600 K and 1000 K, the desorption rate is determined by an interface-diffusion mixed kinetic regime. In steady-state, the desorption flux of deuterium tends towards a diffusion limiting step at low temperature and towards a surface recombination limiting step at high temperature.

In the temperature range investigated during this study (723 K – 773 K), there are both a significant concentration gradient in the oxide and a significant hydrogen surface concentration: around 10 – 20 mol m^{-3} (see Figure 9) in consistency with a mixed kinetic regime. In addition, as expected, the desorption fluxes assessed by simulations for these two experiments (19 days_723 K – 7 days_773 K) are much lower (black crosses) than the steady-state fluxes (blue dotted line).

From the desorption fluxes, the amount deuterium desorbed can be estimated.

5.3.3 Assessment of deuterium amount desorbed in the long term

By integrating the desorption flux with the optimized kinetic constants, the desorbed deuterium amount can be assessed for a 500-days (period of one PWR cycle approximately) exposure time at 573 K, the average in-vessel temperature. The deuterium concentration profile in the oxide layer after such exposure conditions can be simulated as shown on the Figure 15.

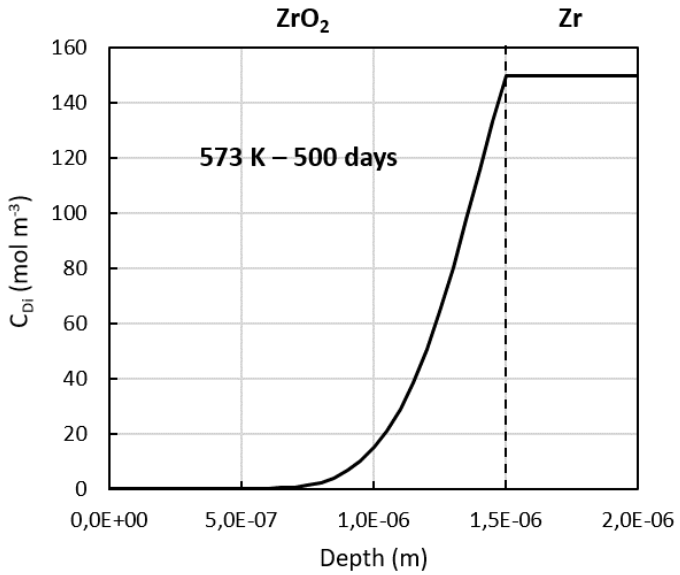

Figure 15. Simulated deuterium concentration profile as function of depth, obtained with the kinetic constants expressed according to Eq.10 and Eq.11, after desorption at 573 K during 500 days.

Figure 14 indicates that, at such temperature, the steady state desorption flux would be in the order of 10^{-14} mol m^{-2} s^{-1}. However, Figure 15 shows a diffusion profile of deuterium in zirconia representative of the transient state. After 500 days at 573 K, the deuterium still failed to reach the surface of the oxide. To tend towards the steady-state, several tens of years would be necessary. Therefore, at 573 K, the deuterium amount released from the alloy through the 1.5 µm-thick zirconia layer is infinitesimal. These calculations represent an upper limit of the deuterium desorbed amounts due to the assumption of the concentration equality in the metal and in the oxide (which is likely less than that in the metal at lower temperature) at the metal/oxide interface. In addition, under operating PWR conditions, the hydrogen absorption process during the water corrosion cannot be neglected, unlike under vacuum. The corresponding hydrogen flux through the oxide is opposed to the deuterium or tritium release from the alloy, which may have an impact on the desorption rate. Moreover, the presence of water molecules adsorbed at the oxide surface may modify the desorption mechanism. Finally, the oxide layer of few nanometers at the beginning grows progressively until it reaches a thickness of 1.8 µm in the pre-transient regime. Beyond this thickness, in post-transient regime, the oxide layer will continue to grow, forming a porous zirconia sub-layer on the surface, which will probably be more permeable to hydrogen.

6 Conclusion

The effect of the presence of a 1.5 µm-thick oxide layer formed during 50 days in light primary water at 633 K and 188 bars on the deuterium desorption from Zircaloy-4 was evaluated through SIMS analysis and by using modelling programed with FE Cast3M code and URANIE optimization tool. Two heat treatments were carried out in vacuum during 7 days at 773 K and during 19 days at 723 K. The results of these researches are consistent with the following conclusions:

1. During the oxidation of the samples, the deuterium present in the metal did not diffuse through the oxide layer.
2. During both studied heat treatments, a concentration gradient of deuterium in the oxide layer appears, revealing the deuterium transport from the metal into the oxide and its diffusion in the oxide towards the external interface. However, during these two isotherms, the deuterium did not desorb in a significant and measurable way.
3. No marked dissolution of the oxide layer formed in light primary water was evidenced after 7 days at 773 K and 19 days at 723 K under vacuum.

4. The kinetic constant k'_{des} of the surface recombination step and the deuterium diffusion coefficient $D_{i_{ox}}^{diff}$ in the oxide layer are expressed as follows:

$$k'_{des} = 7\text{x}10^{-13}\ exp\left(-\frac{34{,}5\ kJ\ mol^{-1}}{RT}\right)\ \text{m}^4\ \text{mol}^{-1}\ \text{s}^{-1} \quad \text{(Eq.10)}$$

$$D_{i_{ox}}^{diff} = 2\text{x}10^{-8}\ exp\left(-\frac{156{,}1\ kJ\ mol^{-1}}{RT}\right)\text{m}^2\ \text{s}^{-1} \quad \text{(Eq.11)}$$

5. The deuterium desorption from an oxidized zirconium alloy is rate-limited by a mixed regime of surface recombination and diffusion in the oxide for a temperature range between 600 K and 1000 K. At lower temperature, the desorption rate is controlled by the deuterium diffusion in the oxide whereas at high temperature the surface recombination step prevails.

7 Acknowledgements

The authors would like to thank Framatome for supplying the studied material and the Alternative Energies and Atomic Energy Commission for supporting this research.

8 Data availability

The raw/processed data required to reproduce these findings cannot be shared at this time as the data also forms part of an ongoing study.

9 References

[1] S. Suman, Mohd.K. Khan, M. Pathak, R.N. Singh, J.K. Chakravartty, Hydrogen in Zircaloy: Mechanism and its impacts, Int. J. Hydrog. Energy. 40 (2015) 5976–5994. https://doi.org/10.1016/j.ijhydene.2015.03.049.

[2] A. Zieliński, S. Sobieszczyk, Hydrogen-enhanced degradation and oxide effects in zirconium alloys for nuclear applications, Int. J. Hydrog. Energy. 36 (2011) 8619–8629.

[3] A.T. Motta, L. Capolungo, L.-Q. Chen, M.N. Cinbiz, M.R. Daymond, D.A. Koss, E. Lacroix, G. Pastore, P.-C.A. Simon, M.R. Tonks, B.D. Wirth, M.A. Zikry, Hydrogen in zirconium alloys: A review, J. Nucl. Mater. 518 (2019) 440–460. https://doi.org/10.1016/j.jnucmat.2019.02.042.

[4] IAEA, Waterside corrosion of zirconium alloys in nuclear power plants, Int. At. Energy Agency. TECDOC-996 (1998).

[5] C. Juillet, M. Tupin, F. Martin, Q. Auzoux, C. Berthinier, F. Miserque, F. Gaudier, Kinetics of hydrogen desorption from Zircaloy-4: Experimental and modelling, Int. J. Hydrog. Energy. 44 (2019) 21264–21278.

[6] C. Juillet, M. Tupin, F. Martin, Q. Auzoux, S. Bosonnet, C. Berthinier, Effect of a pre-oxidation on the hydrogen desorption from Zircaloy-4, Corros. Sci. 173 (2020) 108762.
[7] C. Juillet, M. Tupin, F. Martin, Q. Auzoux, C. Berthinier, F. Gaudier, T. Guilbert, C. Toffolon, Effect of the precipitates on the hydrogen desorption kinetics from zirconium-niobium alloys, Int. J. Hydrog. Energy. 46 (2021) 8113–8124. https://doi.org/10.1016/j.ijhydene.2020.12.025.
[8] M.W. Mallet, W.M. Albrecht, Low-Pressure Solubility and Diffusion of Hydrogen in Zirconium, J. Electrochem. Soc. 104 (1957) 142.
[9] G. Amsel, D. David, G. Beranger, P. Boisot, B. De Gelas, P. Lacombe, Analyse a l'aide d'une methode nucleaire des impuretes introduites dans les metaux par leurs preparations d'etat de surface: Application au zirconium, J. Nucl. Mater. 29 (1969) 144–153.
[10] C.R. Cupp, P. Flubacher, An autoradiographic technique for the study of tritium in metals and its application to diffusion in zirconium at 149° to 240° C, J. Nucl. Mater. 6 (1962) 213–228.
[11] G.U. Greger, H. Münzel, W. Kunz, A. Schwierczinski, Diffusion of tritium in zircaloy-2, J. Nucl. Mater. 88 (1980) 15–22.
[12] A. Sawatzky, The diffusion and solubility of hydrogen in the alpha phase of Zircaloy-2, J. Nucl. Mater. 2 (1960) 62–68.
[13] C. Schwartz, M. Mallet, Observation of the behavior of hydrogen in zirconium, Trans. Am. Soc. Met. 46 (1954) 641–654.
[14] B.F. Kammenzind, D.G. Franklin, H.R. Peters, W.J. Duffin, Hydrogen Pickup and redristribution in alpha annealed Zircaloy-4, Zircon. Nucl. Ind. 11th Int. Symp. ASTM STP 1295. (1996) 338.
[15] C.-S. Zhang, B. Li, P.R. Norton, The study of hydrogen segregation on Zr(0001) and Zr(1010) surfaces by static secondary ion mass spectroscopy, work function, Auger electron spectroscopy and nuclear reaction analysis, J. Alloys Compd. 231 (1995) 354–363.
[16] J.H. Austin, T.S. Elleman, K. Verghese, Tritium diffusion in zircaloy-2 in the temperature range −78 to 204° C, J. Nucl. Mater. 51 (1974) 321–329.
[17] W. Chen, L. Wang, S. Lu, Influence of oxide layer on hydrogen desorption from zirconium hydride, J. Alloys Compd. 469 (2009) 142–145.
[18] W. Kunz, H. Münzel, U. Kunz, Tritium release from Zircaloy-2: Dependence on temperature, surface conditions and composition of surrounding medium, J. Nucl. Mater. 136 (1985) 6–15.
[19] D. Wongsawaeng, S. Jaiyen, High-temperature absolute hydrogen desorption kinetics of zirconium hydride under clean and oxidized surface conditions, J. Nucl. Mater. 403 (2010) 19–24.
[20] W. Kunz, H. Münzel, U. Helfrich, Diffusion of tritium in zircaloy: Influence of low irradiation damage, oxygen concentration and formation of δ-hydrides, J. Nucl. Mater. 105 (1982) 178–183.
[21] K. Une, Kinetics of reaction of Zirconium alloy with hydrogen, J. Common Met. 57 (1978) 93–101.
[22] R.P. Marshall, Absorption of gaseous hydrogen by Zircaloy-2, J. Common Met. 13 (1967) 45–52.
[23] N.S. McIntyre, R.D. Davidson, C.G. Weisener, B.D. Warr, M.B. Elmoselhi, SIMS studies of hydrogen diffusion through oxides on Zr□Nb alloy, Surf. Interface Anal. 17 (1991) 757–763.
[24] K. Park, D.R. Olander, Hydrogen Dissolution in and Release from Nonmetals: III, Tetragonal Zirconia, J. Am. Ceram. Soc. 74 (1991) 72–77.
[25] M. Tupin, F. Martin, C. Bisor, R. Verlet, P. Bossis, J. Chene, F. Jomard, P. Berger, S. Pascal, N. Nuns, Hydrogen diffusion process in the oxides formed on zirconium alloys during corrosion in pressurized water reactor conditions, Corros. Sci. 116 (2017) 1–13.
[26] B. Queylat, Compréhension de l'évolution de la fraction d'hydrogène absorbé par les gaines en alliage de zirconium, École Normale Supérieure Paris-Saclay, 2020.
[27] A. Roustila, J. Chêne, C. Séverac, XPS study of hydrogen and oxygen interactions on the surface of zirconium, J. Alloys Compd. 356–357 (2003) 330–335.
[28] C. Andrieu, Etude de la permeation du tritium à travers les gaines de crayons combustibles type REP, Université de Grenoble, 1998.
[29] C. Andrieu, S. Ravel, G. Ducros, C. Lemaignan, Release of fission tritium through Zircaloy-4 fuel cladding tubes, J. Nucl. Mater. 347 (2005) 12–19.
[30] D. Khatamian, Hydrogen diffusion in oxides formed on surfaces of zirconium alloys, J. Alloys Compd. 253–254 (1997) 471–474.

[31] X. Ma, C. Toffolon-Masclet, T. Guilbert, D. Hamon, J.C. Brachet, Oxidation kinetics and oxygen diffusion in low-tin Zircaloy-4 up to 1523K, J. Nucl. Mater. 377 (2008) 359–369.
[32] www-cast3m.cea.fr/, (n.d.).
[33] F. Gaudier, URANIE: The CEA/DEN Uncertainty and Sensitivity platform, Procedia - Soc. Behav. Sci. 2 (2010) 7660–7661.
[34] M. Tupin, C. Bisor, P. Bossis, J. Chêne, J.L. Bechade, F. Jomard, Mechanism of corrosion of zirconium hydride and impact of precipitated hydrides on the Zircaloy-4 corrosion behaviour, Corros. Sci. 98 (2015) 478–493.

Graphical Abstract

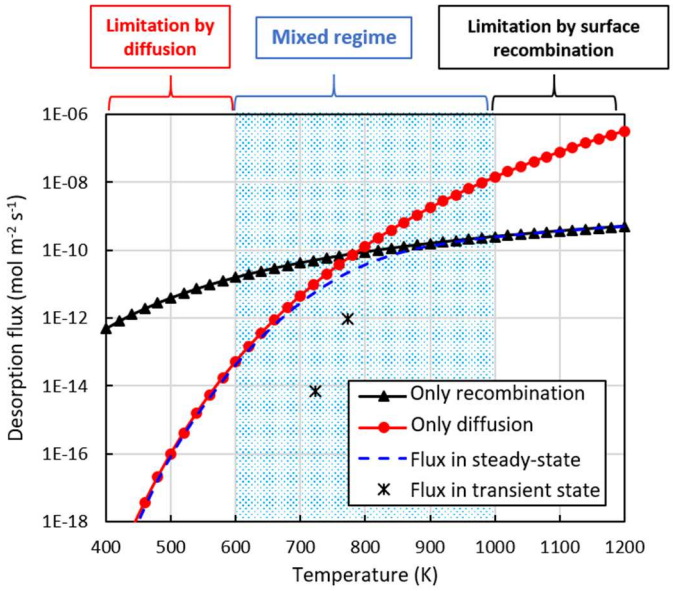

Commissariat à l'énergie atomique et aux énergies alternatives
Centre de Saclay – Bât 458 - pc 15 | 91191 Gif-sur-Yvette Cedex
T. +33 (0)1 69 08 16 27 |
mail :clara.juillet@cea.fr
Etablissement public à caractère industriel et commercial | RCS Paris B 775 685 019

Direction de l'Energie Nucléaire
Direction déléguée aux Activités Nucléaires de Saclay
Département de Physico-Chimie
Service de la Corrosion et du Comportement des Matériaux dans leur Environnement
LABORATOIRE D'ETUDES DE LA CORROSION AQUEUSE